Controlled aggregation of the core(amorphous silica)@shell(TPA-polysilicates) nanoparticles at room temperature by selective removal of TPA^+ (TPA = tetrapropylammonium) ions from the nanoparticle shell

Sanja Bosnar,[a] Maja Dutour Sikirić,[b] Vilko Smrečki,[c] Josip Bronić,[a] Suzana Šegota,[b] Vida Strasser,[b] Tatjana Antonić Jelić,[a] Ana Palčić,[a] and Boris Subotić[*a]

[a]*Laboratory for Synthesis of New Materials, Division of Materials Chemistry, Ruđer Bošković Institute, Bijenička 54, 10000 Zagreb, Croatia. E-mail: sbosnar@irb.hr; bronic@irb.hr; tantonic@irb.hr; Ana.Palcic@irb.hr; subotic@irb.hr*
[b]*NMR Center, Ruđer Bošković Institute, Bijenička 54, 10000 Zagreb, Croatia.E-mail: smrecki@irb.hr*
[c]*Laboratory for Biocolloids and Surface Chemistry, Division of Physical Chemistry, Ruđer Bošković Institute, Bijenička 54, 10 000 Zagreb, Croatia. E-mail: sikiric@irb.hr; ssegota@irb.hr; Vida.Strasser@irb.hr*

Corresponding Author
*E-mail: subotic@irb.hr

ORCID
[b]Maja Dutour Sikirić: 0000-0001-6230-5190
[c]Vilko Smrečki: 0000-0002-0461-5542
[b]Suzana Šegota**:** 0000-0001-6416-3835
[a]Ana Palčić: 0000-0002-1092-4739
[a]Boris Subotić: 0000-0002-3589-7845

ABSTRACT
Investigation (DLS, AFM, pH measurements, ^{29}Si-NMR and ^{23}Na-NMR) of the influence of small inorganic cations (Na^+ ions in this case) on the core@shell silica nanoparticles, formed by room temperature hydrolysis of TEOS in aqueous TPAOH (subsequent addition of NaOH – SA) and NaOH/TPAOH (direct addition of NaOH - DA) solutions showed that the smaller Na^+ ions, displace parts of the larger TPA^+ ions from the shells of the core@shell primary silica nanoparticles (PNPs), by the exchange process and, at the same time, provoke the collisions of the PNPs. These processes enable the binding of the collided nanoparticles by the ≡Si-O-Si≡ bonds (aggregation). The PNPs in the aggregates, formed above the critical aggregation concentration (CAC) of silicate species are separated by the „thick“ shell (TPA-polysilicate anions) that prevents the close contacts between the nanoparticles cores and thus, their coalescence. When Na^+ ions are present during the formation of the nanoparticles, a part of the Na^+ ions is incorporated to the nanoparticle core. Remove of the TPA^+ ions from the shells of the nanoparticles, formed below the CAC, enables close contacts of the nanoparticles cores and thus, their coalescences inside the aggregates. These findings show that the selective removal of the TPA^+ ions from the nanoparticle shell enables the control of the composition and size of the precursor species and thus, represent a good basis for the engineering of nanosized (alumino)silicate microporous and mesoporous materials.

Keywords: core@shell silica nanoparticles, composition of nanoparticle shell, removal of the TPA^+ ions from the nanoparticle core, controlled aggregation of the primary silica nanoparticles, influence of the amount and mode of addition of NaOH on the size and structure of aggregates

Introduction

Although the existence of nanosized zeolites has been well-known since the early days of zeolite synthesis,[1,2] the use of colloidal science principles in the synthesis of the nanosized zeolites was consistently developed by B. J. Schoeman and co-workers during the nineties of the last century.[3-8] Thereafter, many different colloidal, nanosized zeolites such as zeolites A,[3,9-12] FAU (X, Y),[3,9,11] L,[12,13] hydroxysodalite,[7] beta,[11,12,14-17] $AlPO_4$-5,[18] MEL,[19], EMT,[20] SSZ-13,[21] ZSM-5[4,12,22] and especially silicalite-1[5,6,22-38] were successfully synthesized by many research groups over the world.

The success in the synthesis of different types of colloidal, nanosized zeolites was followed by the finding out that the process of crystallization starts by the formation of very small, 2 – 5 nm sized, sub-colloidal particles which are in the reaction mixture present during the entire process of crystallization.[5,6,25,29-32] Thus, the investigation of the formation of sub-colloidal (nano-sized) TAA-(alumino)silicate (TAA = tetra alkyl ammonium) particles[5,21,23,25-34,39] and their evolution during either room-temperature ageing[26,29,33] and/or hydrothermal treatment[5,21,23-28,30-33] of the homogeneous reaction mixtures [HmRMs; initially clear TAA-(alumino)silicate solutions] was, for the long time, and still is, one of the most provocative objectives in the field of zeolite crystallization. Results of these investigations indicated that the formation of the "primary units" (primary nanoparticles – PNPs), having the size of about 2 – 5 nm,[5,21,23,25,27-29,31,34] is the critical step in the crystallization of zeolites in both homogeneous (HmRMs)[5,21,23,25,27-29,31] and heterogeneous (HtRMs)[23,40-45] reaction mixtures (RMs). For these reasons, great attempts were made to elucidate the "structure" and properties of the sub-colloidal particles and their role in zeolite crystallization.[5,6,11,23-25,27-32,34-46]

On the basis of numerous studies of the formation of silica nanoparticles in homogeneous systems TEOS-TAAOH-H_2O,[27,34,47-50] it was concluded that silica-TAAOH solutions have

well defined critical aggregation concentration (CAC) of silica for OH^-/SiO_2 = TAAOH/TEOS ≈ 1. Many studies[21,27,30,34,47-50] suggest that prior to this critical point (below the CAC; OH^-/SiO_2 > 1) the solution (HmRM) contains only silicate monomers and polysilicate anions (oligomers). In spite of widely spread meaning that the silica nanoparticles cannot be formed below the CAC,[15,16,21,27,30,35,47-49,51] our recent study resolute evidenced the formation of stable, about 1 - 2 nm-sized core(amorphous SiO_2)@shell(TPA^+ ions) nanoparticles, below the CAC.[52]

Earlier models of the sub-colloidal PNPs included about 5 nm-sized globular units (GUs) composed of several tetrapods, that may be either amorphous or crystalline[40] and about 3 nm-sized, predominantly amorphous primary precursor species (PPSs), formed by aggregation of several inorganic-organic composite species.[25,36,42] Both these models assume homogeneous distribution of TAA^+ ions in the nanoparticle.

Although these models are attractive and, at the first sight, logical, however, a combination of small-angle X-ray scattering (SAXS) and small-angle neutron scattering (SANS) analyzes[29,35,47,48,50] showed that the silica nanoparticles, formed in the presence of TAA^+ ions, have a core@shell structure with amorphous silica at the core and organic molecules at the shell. The core@shell structure of TAA-amorphous nanoparticles was also identified by computational methods.[53-55] In addition, the independence of the core size and shape upon changes in the cation size is a good indication that the core is mostly cation free.[48,54] The core(amorphous silica)@shell(TAA^+) nanoparticles are stable at room temperature for long time.[5,25-30,48]

Very often, the nanoparticle shell is considered as organic cations (Org^{n+}), usually tetraalkylammonium (TAA^+) and most frequently, TPA^+ ions, adsorbed on the surface of SiO_2 nanoparticle core.[17,27-29,35,37,53,55,56] This consideration includes association of the Org^{n+} (TAA^+, TPA^+) ions with deprotonated silanol groups[37] and formation of a Stern layer of the

adsorbed cations, that is effectively part of the liquid phase of the system.[27,35] On the other hand, our recent investigation of the processes occurring during early stages of the formation and room temperature (*rt*) evolution of the core(amorphous SiO_2)@shell(organocations) nanoparticles has shown that, above the CAC ($OH^-/SiO_2 < 1$), the nanoparticle shell is formed by attachment of the polysilicate anions (silicate oligomers), associated with TPA^+ ions, on the surfaces of the nanoparticles cores.[52] This gives a new insight in the "structure" of the nanoparticle shell, which is considerably different from the most frequently described one, i.e., "free" TPA^+ ions adsorbed on the surface of the nanoparticle core,[17,21,27-29,34,35,37,48,50,53,55,56] as it is also characteristic for the nanoparticles formed below the CAC.[52] This, at the same time, requires the re-consideration of the interaction of the nanoparticles during room-temperature aging, especially in the presence of alkali metal cations which can displace the TAA^+ ions[57] from nanoparticle shell.

In spite of the fact that the *rt* evolution of the nanoparticles in the presence of alkaline cations (mostly Na^+ ions), strongly influences the pathways of zeolite crystallization in both HmRMs[4,25,33,38] and HtRMs,[40,43-45] the influence of concentration of Na^+ and/or other alkali cations on the *rt* evolution of the silica nanoparticles in homogeneous systems, is hardly studied.[47,48,58] For this reason, the objective of this work is the study of the influence of the concentration of the Na^+ ions, added into reaction mixture during and/or after formation of the core@shell PNPs on the processes of their aggregation and on the characteristics of the obtained aggregates. The obtained results are correlated with the characteristics and "structure" of the nanoparticle shell and specific interactions of the Na^+ ions, added into HmRMs, and TPA^+ ions from the shell.

Experimental

Preparation and treatment of the homogeneous reaction mixtures (HmRMs)

The investigated homogeneous reaction mixtures (HmRMs) having the batch molar compositions: nSiO$_2$:xNaOH:(0.36 – x)TPAOH:4nEtOH:18H$_2$O were prepared in two ways, with respect to the addition of NaOH:

1. Subsequent addition of NaOH:

a) n = 1: NaOH-free reaction mixtures (1a-RMs), having the initial chemical composition: TEOS:(0.36 – x_s)TPAOH:(20 – y)H$_2$O (x = x_s = 0 - 0.018 and y is the amount of water which is subsequently added in the form of 3.846 wt. % NaOH solution) were prepared at room temperature (*rt*) by adding the appropriate amounts of tetraethylorthosilicate (TEOS, Aldrich, 98 %, reagent grade) to a water solution of tetrapropylammonium hydroxide (TPAOH, 1M aqueous solution, Alfa Aesar). For this purpose, the appropriate amount (mass) of TEOS was quickly added into a plastic vessel containing appropriate amount of TPAOH solution stirred by magnetic bar. Such prepared RMs were stirred for t_s = 60 min. During this time, TEOS was completely hydrolysed, which resulted in the formation of the clear solutions (homogeneous reaction mixtures – 1a-HmRMs) having the batch molar composition: SiO$_2$:(0.36 – x_s)TPAOH:4EtOH:(18 – y)H$_2$O at $t_s \leq 60$ min. Then, an appropriate amount (mass) of 3.846 wt. % NaOH solutions was added to the prepared clear solution. The newly formed HmRMs (1aS-HmRMs) having the chemical compositions: SiO$_2$:x_sNaOH(0.36 - x_s)TPAOH:4EtOH:18H$_2$O, characterized by the values of x_s and R_s = x_s/0.36, were stirred (aged) at *rt* for $t_{s'}$ = 40, 80 and 120 min and then, additionally aged, under static conditions, for $t_{a'} \geq 22$ h, so that $t_{A'} = t_{s'} + t_{a'} \geq 24$ h. The moment of addition of TEOS into TPAOH solution was taken as the zero time, (t_s = 0) of the hydrolysis process, and the moment of addition of NaOH solution into NaOH-free HmRM was taken as the zero time ($t_{s'}$ = 0) of the *rt* stirring of NaOH-containing HmRM.

b) n = 0.2: NaOH-free reaction mixture (1b-RM), having the initial chemical composition: 0.2TEOS:0.3528TPAOH:18.45H_2O was prepared at room temperature (*rt*) by adding the appropriate amounts of TEOS (Aldrich, 98 %, reagent grade) to a water solution of TPAOH (1M aqueous solution, Alfa Aesar). For this purpose, the appropriate amount (mass) of TEOS was quickly added into a plastic vessel containing appropriate amount of TPAOH solution stirred by magnetic bar. Such prepared RM was stirred for t_s = 60 min. During this time, TEOS was completely hydrolysed, which resulted in the formation of the clear solution (homogeneous reaction mixture – 1b-HmRM) having the batch molar composition: 0.2SiO_2:0.3528TPAOH:0.8EtOH:18.05H_2O. Addition of an appropriate amount (mass) of 1 wt. % NaOH solution into 1b-HmRm resulted in NaOH-containing 1bS-HmRM (0.2SiO_2:0.0072NaOH:0.3582TPAOH:0.8EtOH:19.6H_2O). The newly formed 1bS-HmRM was stirred 2 h and then, additionally aged, under static conditions, for 22 h, so that $t_{A'} = t_{s'} + t_{a'}$ = 24 h, before the characterization. The moment of addition of TEOS into TPAOH solution was taken as the zero time, (t_s = 0) of the hydrolysis process, and the moment of addition of NaOH to 1b-HmRM was taken as the zero time ($t_{s'}$ = 0) of the *rt* stirring of 1bS-HmRM.

<u>2. Direct addition of NaOH</u>: The investigated homogeneous reaction mixtures, 2-RMs, having the initial chemical compositions: TEOS:x_dNaOH:(0.36 - x_d)TPAOH:20H_2O (x_d = 0.018 – 0.054; $R_d = x_d/0.36$ = 0.05 - 015), were prepared at room temperature (*rt*) by adding the appropriate amounts of TEOS to water solutions, containing the appropriate amounts of TPAOH and NaOH; the molality concentrations [NaOH], [TPAOH] and [H_2O] of NaOH, TPAOH and H_2O were determined by the relationships: [NaOH]:[TPAOH]:[H_2O] = x_d:(0.36 – x_d):20 and {[NaOH] + [TPAOH]}:[H_2O] = 0.36:20. For this purpose, the appropriate amount (mass) of TEOS was quickly added into a plastic vessel containing appropriate amount of (NaOH, TPAOH) solution stirred by magnetic bar. Such prepared, 2-RMs, were stirred (aged)

at *rt* for t_s = 40, 80 and 120 min and then, additionally aged, under static conditions, for $t_a \geq 22$ h, so that $t_s + t_a \geq 24$ h. Note that, after the complete hydrolysis (2-RMs -> 2D-HmRMs), the chemical composition of such prepared 2D-HmRMs is: SiO_2:x_dNaOH:(0.36 – x_d)TPAOH:4EtOH:18H_2O, and is characterized by the values of x_d and $R_d = x_d/0.36$. The moment of addition of TEOS into (NaOH,TPAOH) solution was taken as the zero time, (t_s = 0) of the hydrolysis/aging processes.

The "control", NaOH-free HmRMs: SiO_2:0.36TPAOH:4EtOH:18H_2O ($HmRM_0$-I) and 0.2SiO_2:0.36TPAOH:0.8EtOH:19.6H_2O ($HmRM_0$-II) were prepared by quick addition of appropriate amounts of TEOS into the plastic vessels containing appropriate amounts of water solutions of TPAOH, stirred by magnetic bar for t_s = 2 h and then, additionally aged for t_a = 22 h ($t_A = t_s + t_a$ = 24 h). The preparation, stirring and aging of the "control" HmRMs were performed at room temperature.

Characterization

The pH of the HmRMs, prepared by both subsequent addition of NaOH (1bS-HmRMs) and direct addition of NaOH (2D-HmRMs), including the "control" homogeneous reaction mixture ($HmRM_0$-I) were measured at the time $t_{A'}$= 24 h for the 1bS-HmRMs and at t_A = 24 h for the 2D-HmRMs. The pH of the HmRMs was measured using a Corning Pinnacle 555 pH/ion meter. The pH meter was calibrated with pH 9.0 and 12.0 buffer solutions at 25 °C. The accuracy of the pH meter was ±0.01 pH units

The size distributions of the nanoparticles formed/present in the investigated HmRMs (1aS-HmRMs, 1bS-HmRMs, 2D-HmRMs, $HmRM_0$-I and $HmRM_0$-II) were determined by means dynamic light scattering (DLS), using a photon correlator spectrophotometer equipped with a 532 nm "green" laser (Zetasizer Nano ZS, Malvern Instruments, UK). Intensity of scattered light was detected at the angle of 173°. To avoid overestimation arising from the scattering of larger particles, the hydrodynamic diameter (D_h) was obtained as a value at peak

maximum of size number distribution function. The size distributions of the nanoparticles in the investigated HmRMs were measured after *rt* stirring for $t_{s'}(t_s)$ = 40, 80 and 120 min and after additional *rt* ageing, under static conditions, for $t_{a'}(t_a)$, so that $t_{A'} = (t_{s'} + t_{a'}) \geq 24$ h and $t_A = (t_s + t_a) \geq 24$ h. Each sample was measured 10 times and the results were expressed as the average value. All measurements were conducted at 25 ± 0.1 °C. The data processing was done by Zetasizer software 6.32 (Malvern instruments).

AFM imaging of the nanoparticles present in the investigated HmRMs was performed in soft tapping mode using a MultiMode Scanning Probe Microscope with a Nanoscope IIIa controller (Bruker, Billerica, USA) with a vertical engagement (JV) 125 mm scanner. For this purpose, 5 μL of each of the selected HmRMs stirred/aged at *rt* for $t_A(t_{A'})$ = 24 h, was pipetted directly onto mica substrate and incubated for 10 min. Then, the excess of the HmRM was removed from the substrate by filter paper and the mica sheets were placed in enclosed Petri dishes for several hours at a relative humidity of up to 50% to evaporate the excess water. The NanoScope was allowed to equilibrate thermally for 1 h before imaging. Scanning rates were normally optimized around 1 Hz at a scan angle of 90° Images were recorded under ambient conditions in air, by using silicon tips (RTESP, Bruker, nom. freq. 320 nom. freq. 320 kHz, nom. spring constant of 42 Nm1). Images were processed and analysed by means of the offline AFM NanoScopeTM software (Digital Instruments, Version 5.12r5, Digital Instruments, Tonawanda, NY, USA). All images are presented as raw data except for the first-order two-dimensional flattening. Since the AFM height and lateral resolution is under 1 nm, and the curvature radius of the sharp AFM probe is below 8 nm, it could be used to characterize the small difference of the surface morphology and the dimensions of aggregates.

All ^{29}Si and ^{23}Na NMR experiments were carried out on a Bruker Avance 600 spectrometer (600.13 MHz, ^{1}H; 158.75 MHz, ^{23}Na; 119.22 MHz, ^{29}Si). Samples were measured in 5 mm NMR tubes at 293 K. A sealed 2 mm glass capillary filled with 0.1 M NaCl

in D_2O was inserted into the tube prior to measurement and served as an internal reference for chemical shifts in parts per million. ^{23}Na and ^{29}Si spectra were recorded in a broadband-observed (BBO; BB, ^{1}H; inner coil tuned for ^{23}Na and ^{29}Si, respectively) probe with a built-in z-gradient coil. Typically, ^{29}Si spectra at a spectral width of 50 kHz and a digital resolution of 1.5 Hz per point were measured with 2048 scans. A 90° pulse was used with a repetition rate of 7 s. ^{23}Na spectra were measured with 256 scans at a spectral width of 20 kHz and a digital resolution of 0.5 Hz per point. A 90° pulse was used with a repetition rate of 1 s. All experimental data were zero-filled to double the number of experimental points and then baseline-corrected using automatic baseline correction. The software TopSpin (Bruker BioSpin) version 2.1 was used for all acquisition and processing. ^{29}Si NMR quantification was performed by spectral deconvolution using the Dmfit software.[59]

Results and discussion

The particle size distribution (DLS-PSD curves in Fig. 1A) show that the nanoparticles formed by the *rt* hydrolysis of TEOS in the absence of NaOH (HmRM = $HmRM_0$-I: SiO_2:0.36TPAOH:4EtOH:18H_2O, see Experimental), and aged at *rt* for t_A = 24 h (see Methods as well as the considerations in the Supporting Information SI-1), represent the individual PNPs having the sizes in the range from $D_{min} \approx 1$ nm to $D_{max} \approx 3.6$ nm with $D_p(N) = 1.74$ nm [solid curve in Fig. 1A; $D_p(N)$ is the „peak“ size in the PSD by number.].

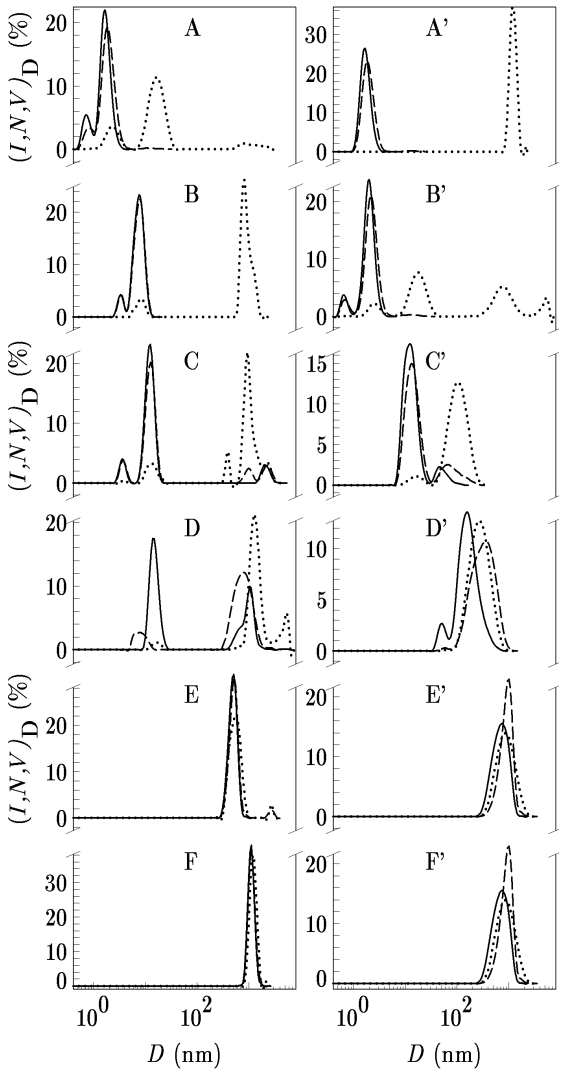

Fig. 1 DLS-PSDs by number (N_D vs. D; solid curves), volume (V_D vs. D; dashed curves) and intensity (I_D vs. D; dotted curves) in the HmRMs: SiO_2:0.36TPAOH:4EtOH:18H_2O (A) and SiO_2:xNaOH(0.36 – x)TPAOH:4EtOH:18H_2O characterized by: (B) $x = x_s = 0.0018$; (C) $x = x_s = 0.0036$; (D) $x = x_s = 0.0108$; (E) $x = x_s = 0.0144$; (F) $x = x_s = 0.018$; (A') $x = x_d = 0.018$; (B') $x = x_d = 0.027$; (C') $x = x_d = 0.036$; (D') $x = x_d = 0.0396$; (E') $x = x_d = 0.0468$ and (F') $x = x_d = 0.054$. All the investigated HmRMs were prepared by the procedures described in Experimental and stirred/aged at room temperature for $t_{A'} = t_{s'} + t_{a'} = 24$ h and/or $t_A = t_s + t_a = 24$ h (see Experimental) before analyses. N_D is the number percentage, V_D is the volume (mass) percentage and I_D is the scattering intensity percentage of the particles having the spherical equivalent diameter D. The meanings of $x = x_s$, $x = x_d$, $t_{A'}$, $t_{s'}$, $t_{a'}$, t_A, t_s and t_a are explained in Experimental and further in the text.

The AFM topographic image in Fig. 2A clearly shows that the single (individual) nanoparticles, formed in the NaOH-free $HmRM_0$-I are deposited on mica surface during the preparation of samples for the AFM imaging (see Experimental). The AFM cross-section

analysis (Fig. 2A'), along the line of the corresponding topographic 3D height image of the surface layer of nanoparticles on mica support, show that the nanoparticles heights lie in the range from about 1 nm to about 2 nm, which is consistent with the results of the DLS analysis.

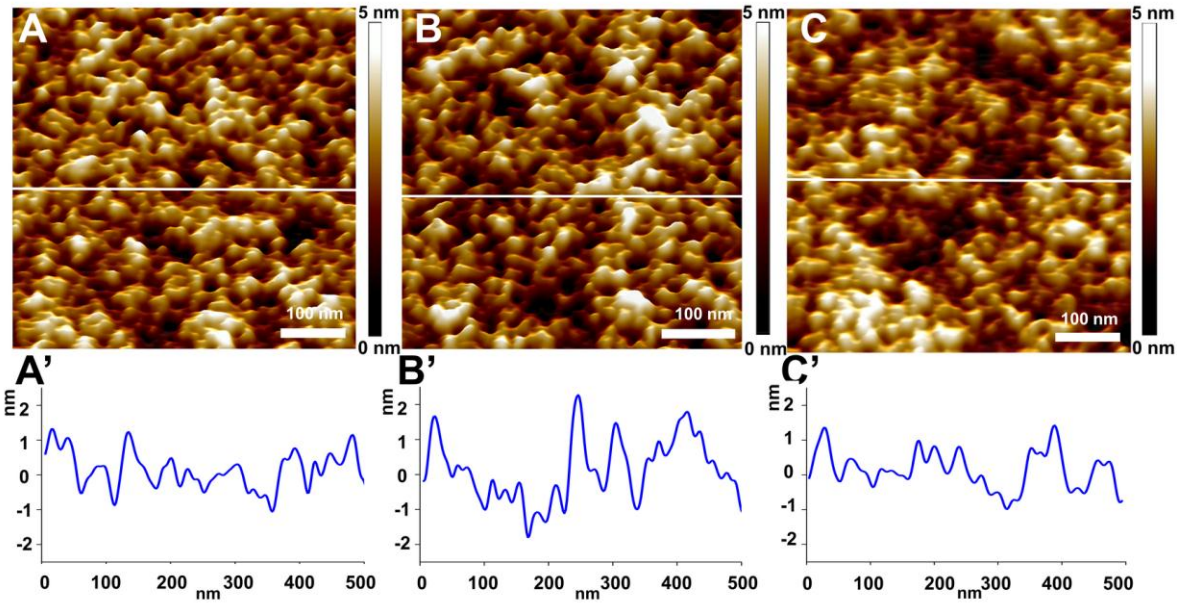

Fig. 2 AFM topographic images (A, B, C) and the corresponding section analyses (A', B', C') of the nanoparticles in the HmRMs: SiO_2:0.36TPAOH:4EtOH:18H_2O ($HmRM_0$-I; A, A'); and SiO_2:xNaOH(0.36 – x)TPAOH:4EtOH:18H_2O characterized by: $x = x_s = 0.0144$ (1aS-HmRM; B, B') and x = x_d = 0.0468 (2D-HmRM; C, C'). The images are presented as 3D height data (A, B, C) and the cross-section through the line shown on the same scale (A', B', C'): scan size of 500 nm × 500 nm and vertical scale of 5 nm. The investigated HmRMs were prepared by the procedures described in Experimental and stirred/aged at room temperature for $t_{A'} = t_{s'} + t_{a'}$ = 24 h and/or $t_A = t_s + t_a$ = 24 h (see Experimental). The meanings of $x = x_s$, $x = x_d$, $t_{A'}$, $t_{s'}$, $t_{a'}$, t_A, t_s and t_a are explained in Experimental and further in the text.

Since the nanoparticles have not been observed in the "blank" samples (0.694 M solution of TPAOH),[52] it is evident that AFM 3D-height images (Fig. 2A– 2C) confirm the presence of the PNPs which have the relative narrow height distribution, ranging from 1 to 2 nm.

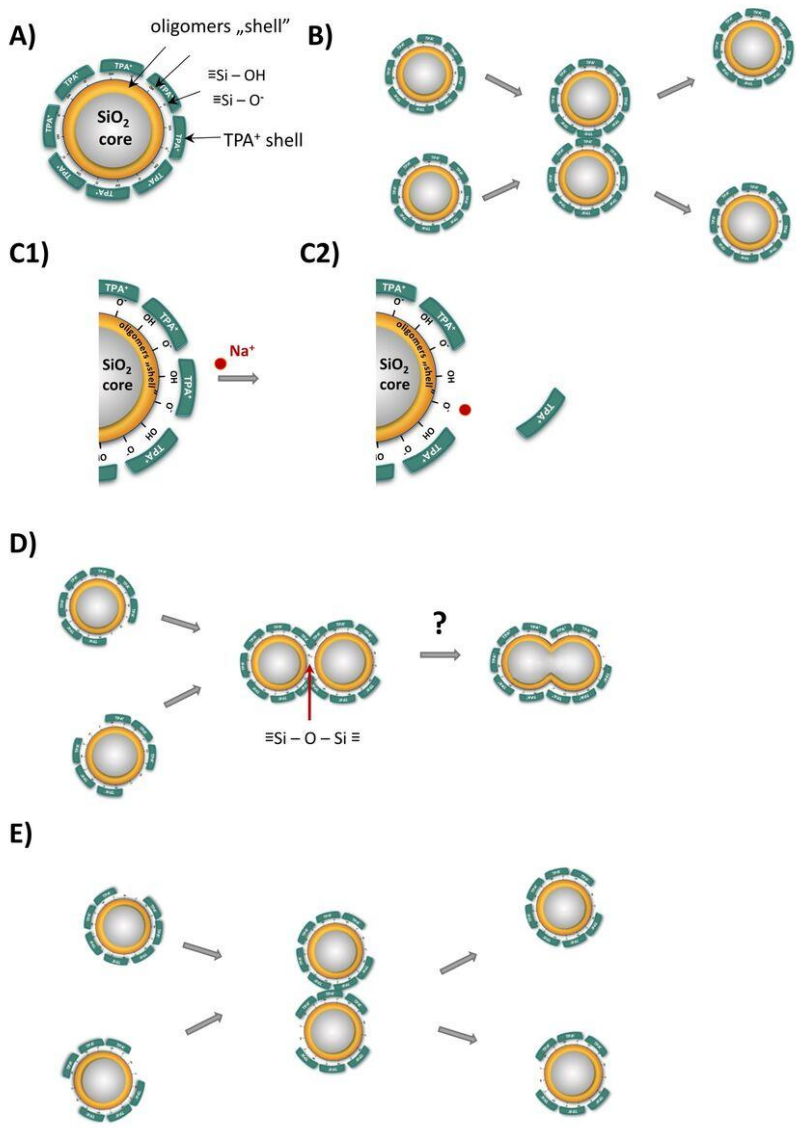

Scheme 1 Schematic presentation of the behaviour of the primary nanoparticles (PNPs) in Na^+-free $HmRM_0$-I (A, B) and in the 1aS-HmRMs after subsequently added NaOH (C – E), during *rt* stirring/ageing of the corresponding HmRMs. Details are explained in the text. The relationship between the SiO_2 core and the shell is, from practical reason, simplified in the way explained in SI-3.

Figure 1A and Figure S1 in SI-2 show that the PNPs, formed in $HmRM_0$-I, are stable for at least 37 days, which is consistent with the results of previous investigation.[49] Taking into consideration that the PNPs have the core@shell structure,[9,21,27-29,34,35,47,48,50,56] it is reasonable to assume that this stability is connected not only with the negative charge of the

PNPs,[31,35,50,60] but also with overlapping of the terminal silanol groups (PNP≡Si-OH and PNP≡Si-O^-) with TPA^+ ions (see Scheme 1A; also see Scheme S1 in SI-3). Negative charge of the PNPs, arising from both internal (bulk)[50] and external (surface) deprotonated silanol groups (≡Si-O^-)[31,35,50,60] (see Schemes 1A and 1C; also see Scheme S1 in SI-3), causes repulsive force between neighbouring, potentially colliding PNPs and thus, reduces the collision frequency. On the other hand, since it is reasonable to assume that the TPA^+ ions overlay not only the directly interacting silanol groups of the attached oligomers, but also the surrounding ones,[52] the overlapping ("hiding") of the terminal silanol groups (PNP≡Si-OH and PNP≡Si-O^-) with TPA^+ ions (see Scheme 1C; also see Scheme S1 in SI-3), prevents the reaction,

$$\text{PNP}\equiv\text{Si-OH} + \text{HO-Si}\equiv\text{PNP} \longrightarrow \text{PNP}\equiv\text{Si-O-Si}\equiv\text{PNP} + H_2O \qquad (1)$$

and thus, the formation of ≡Si-O-Si≡ bridges between the collided PNPs. The result is repulsion of the PNPs after each ineffective collision (see Scheme 1B). Hence, it is evident that in this way, the stability of the PNPs is caused not only by electrostatic,[31,35,50,60] but also by steric reasons.[8,29,50,60,61]

In spite of high stability of the PNPs in the NaOH-free $HmRM_0$-I ($x_s = x_d = 0$, $R_s = R_d = 0$; see Methods), subsequent addition of very small amount of sodium hydroxide ($x_s = 0.0018$, $R_s = x_s/0.36 = 0.005$) to the corresponding NaOH-free 1a-HmRMs (see Experimental), causes immediate increase of particles size (see Fig. S2A in SI-2). The consequence is that, 24 h after addition of sodium hydroxide to the NaOH-free 1a-HmRMs ($t_{A'} = 24$ h; see Experimental), the resulting nanoparticles exist as two particles populations; about 10 % of particles have the sizes in the range from D_{min}(N) = 2.7 nm to D_{max}(N) = 4.2 nm with D_p(N) = 3.1 nm and about

90 % of particles (dominant particle population) have the size in the range from D_{min}(N) = 4.9 nm to D_{max}(N) = 13.5 nm with D_p(N) = 7.5 nm (see Fig. 1B). Figs. 1B – 1D show that the increase of x_s from x_s = 0.0018 (R_S = 0.005) to x_s = 0.0108 (R_S = 0.03) does not considerably change the DLS-PSD by number, established at $t_{A'}$ = 24 h. Further increase of the fraction of the subsequently added NaOH causes the formation of large sub-micrometre sized particles with D_p(N) ≈ 500 nm for x_s = 0.0144 at $t_{A'}$ = 24 h (Fig.1E) and even micrometre-sized particles with D_p(N) ≈ 1000 nm for x_s = 0.018 at $t_{A'}$ = 24 h (Fig. 1F).

However, more interesting and important is that the particle size distribution, presented by the solid curves in Figs. 1B – 1F, does not represent the distributions of individual (discrete) particles of different sizes, but rather the aggregates of smaller, individual nanoparticles (PNPs), as can be seen in Figs. 2B and 2B'. The AFM cross section analyses (Fig. 2B'), along the lines of the corresponding topographic 3D height image (Fig. 2B) show that the individual nanoparticles have a relative narrow height distribution ranging from about 1 to 2 nm, which is characteristic for PNPs. Hence, it is evident that the particles larger than PNPs (Figs. 1B – 1D), including the ca. 300 to ca. 1000 nm-sized particles (Figs. 1E and 1 F), measured by DLS, represent aggregates of 1 – 2 nm-sized PNPs.

As expected,[27,35,47,48,50,52,61] the values of pH (and consequently, concentrations of OH^- ions) of the HmRMs aged at *rt* for $t_{A'}$ = 24 h, reached the „equilibrium“ values $pH_{x,24h}$ and $[OH^-]_{x,24h}$ (see Table S1 in SI-1); the „equilibrium“ values do not considerably depend on *x*, because of the reasons explained in SI-1.

As already has been pointed out in the Introduction, the entire amount of silica, formed by hydrolysis of TEOS exists as a mixture of monomers and oligomers below the CAC of silica, and as a mixture of monomers, oligomers, and nanoparticles above the CAC.[14,16,21,34,35,46-48,50,52,56,62] Identification of different silicate species (monomers, oligomers, and nanoparticles) and Si−O−Si connectivity (expressed as Q^n, where *n* is number of bridging

oxygen atoms per SiO_4) in the TEOS−Org$(OH)_n$−H_2O HmRMs (clear solutions) was most frequently carried by ^{29}Si NMR spectroscopy.[14-16,21,30,46,49,51,52]

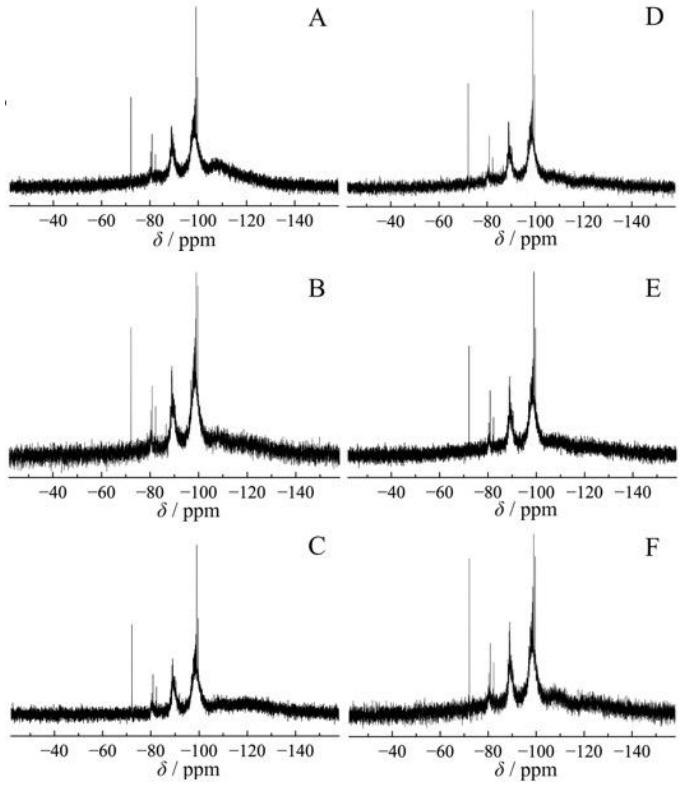

Fig. 3 ^{29}Si-NMR spectra of the HmRMs (clear solution): SiO_2:0.36TPAOH:4EtOH:18H_2O ($HmRM_0$-I; A) and SiO_2:xNaOH(0.36 – x)TPAOH:4EtOH:18H_2O characterized by: $x = x_s$ = 0.0036 (1aS-HmRM; B), $x = x_s$ = 0.0144, (2D-HmRM; C), $x = x_d$ = 0.027, (2D-HmRM; D), $x = x_d$ = 0.036 and (2D-HmRM; E) and $x = x_d$ = 0.0468 (2D-HmRM; F). The investigated HmRMs were prepared by the procedures described in Experimental and stirred/aged at room temperature for $t_{A'} = t_{s'} + t_{a'}$ = 24 h (B, C) and/or $t_A = t_s + t_a$ = 24 h (A, D, E, F; see Experimental) before analyses. The meanings of $x = x_s$, $x = x_d$, $t_{A'}$, $t_{s'}$, $t_{a'}$, t_A, t_s and t_a are explained in Experimental and further in the text.

Figure 3A shows the ^{29}Si-NMR spectrum of the NaOH-free HmRM ($HmRM_0$-I), Figs. 3B and 3C show the ^{29}Si-NMR spectra of the selected 1aS-HmRMs and Figs. 3D – 3F show the ^{29}Si-NMR spectra of the selected 2D-HmRMs (see Experimental for all reaction mixtures). The sharp lines are characteristic of small dissolved silicate oligomers and broader lines are caused by the distributed local silicon environment of nanosized particles.[15,16,21,30,46,49,52] The spectra are quantitatively analysed (see Experimental) in order to determine the distribution of Si in

the form of oligomers and distribution of Si-O-Si connectives in nanoparticles. All the ^{29}Si-NMR spectra, presented in Fig. 3, are similar each to others, and the results of their analyses are consistent with the results of previous investigations. [15,16,21,30,46,49] For these reasons, the results are presented in Tables S2 –S5 in SI-4, and some specific points are commented in SI-4.

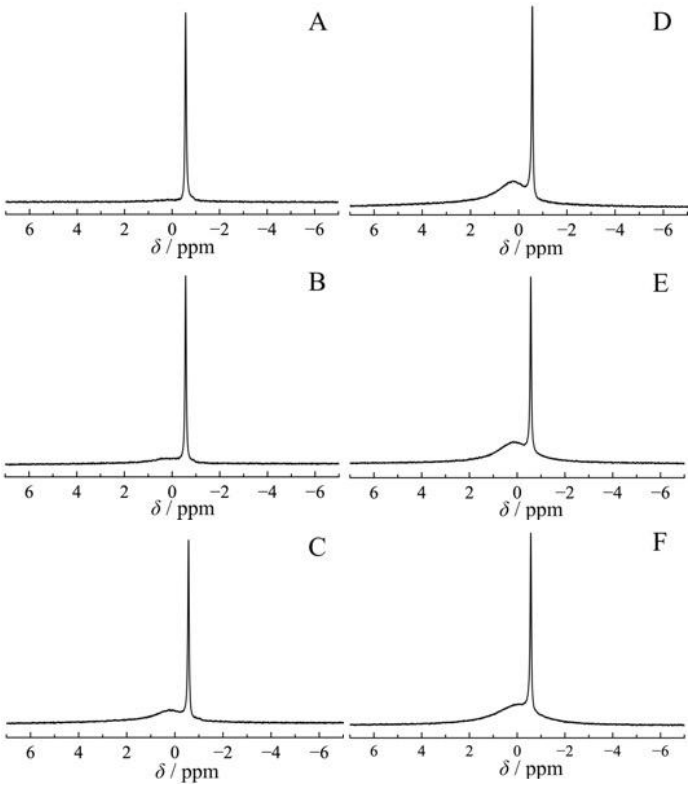

Fig. 4 ^{23}Na-NMR spectra of the HmRMs (clear solution): SiO_2:0.36TPAOH:4EtOH:18H_2O ($HmRM_0$-I; A) and SiO_2:xNaOH(0.36 – x)TPAOH:4EtOH:18H_2O characterized by: $x = x_s$ = 0.0036, (1aS-HmRM; B), $x = x_s$ = 0.0144, (1aS-HmRM; C), $x = x_d$ = 0.027, (2D-HmRM; D), $x = x_d$ = 0.036 (2D-HmRM; E) and $x = x_d$ = 0.0468 (2D-HmRM; F). The sharp lines at δ = -0.57 ppm are relevant for the internal reference (0.1 M NaCl). The investigated HmRMs were prepared by the procedures described in Experimental and stirred/aged at room temperature for $t_{A'} = t_{s'} + t_{a'}$ = 24 h and/or $t_A = t_s + t_a$ = 24 h (see Experimental) before analyses. The meanings of $x = x_s$, $x = x_d$, $t_{A'}$, $t_{s'}$, $t_{a'}$, t_A, t_s and t_a are explained in Experimental and further in the text.

The ^{23}Na-NMR spectrum (Fig. 4A) of NaOH-free $HmRM_0$-I (x = 0, R = 0) shows, as expected, only the sharp line at δ = -0.57 ppm, relevant for the internal reference (0.1 M

NaCl). Subsequent addition of very small amount of NaOH ($x = x_s = 0.0036$, $R = R_s = 0.01$) causes appearance of a broad line in the range from $\delta \approx 1.5$ ppm to $\delta \approx -1.5$ ppm with the "peak" at 0.2 ppm (Fig. 4B). Increase of the amount of the subsequently added NaOH from $x = x_s = 0.0036$ to $x = x_s = 0.0144$, ($R = R_s = 0.04$) increases the intensity of the broad line, but does not change its position (Fig. 4C). Since ^{23}Na is a quadrupolar nucleus with a spin quantum number of 3/2, the ^{23}Na chemical shift is sensitive to the local coordination environment.[63] The observed broadening in Figs. 4B and 4C is therefore most probably caused by a rapid quadrupolar relaxation. It also indicates a higher degree of asymmetry around sodium ions in the nanoparticle shell and/or nanoparticle core.

On the basis of the presented results it is reasonable to postulate that the Na^+ ions from the subsequently added sodium hydroxide remove the TPA^+ ions from the nanoparticle shell (TPA^+-bearing oligomers; see Scheme S1 in SI-3) by the ion exchange process as it is schematically presented in Scheme 1C. This is consistent with the finding that the added alkali metal cations (M^+), having comparatively high surface charge densities, displace TTA^+ from association with polysilicate anions.[57] The mentioned exchange process causes exposition of a part of the terminal silanol groups to the liquid phase and thus, makes them disposable for the reactions described by Eq. (1). However, even in this case, only the collisions at the specific sites (uncovered terminal silanol groups; see Scheme 1C2) of the nanoparticles realizes the establishing of the ≡Si-O-Si≡ bridges between the collided nanoparticles (PPSs) and thus, formation of their aggregates (see Scheme 1D); otherwise, the result is ineffective collision and repulsion of the collided PPSs (see Scheme 1E). Of course, number of the effective collisions, which result in the formation of ≡Si-O-Si≡ bridges between the collided nanoparticles, increases with increased fraction of the uncovered terminal silanol groups. This is, at the same time, the reason that both the size of aggregates (see Figs. 1A - 1F) and the rate of aggregation (see Figs. S2 – S6 in SI-2) increases with increasing amount of the

subsequently added NaOH, expressed by the corresponding values of x_s and R_s. The absence of coalescence of the linked PNPs (see Figures 2B and 2B' as well as Scheme 1D) will be explained later.

From the results presented in Figs. 1B, 1C and 1D and Figs. S2 – S5 in SI-2 it is evident that although the particles (aggregates), existing in different 1aS-HmRMs (R_s = 0.005, R_s = 0.01, R_s = 0.02 and R_s = 0.03), have almost the same size at $t_{A'}$ = 24 h [D_p(N) ≈ 10 nm; see Figs. S2B, S3D, S4D and S5C in SI-2], the "history" of the formation of these particles (aggregates) is different, as it is shown in SI-2.

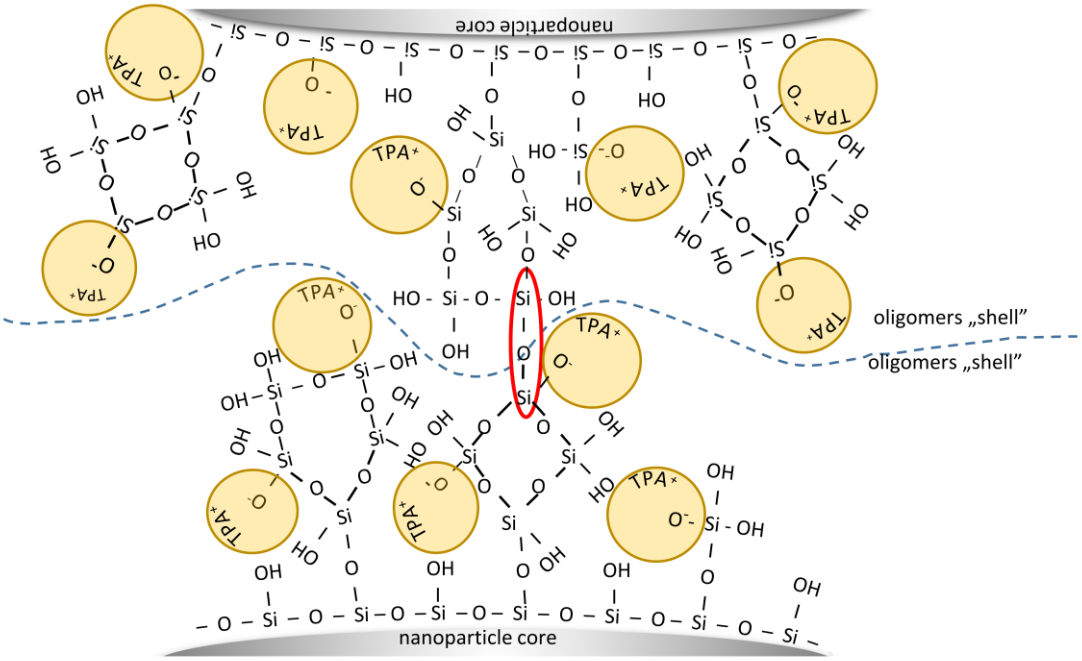

Scheme 2 Schematic presentation of the linking of primary nanoparticles (PNPs) in aggregates. The ≡Si-O-Si-≡ linkage between two neighbouring PNPs is marked by red ellipse

As already has been discussed, exchange of a part of TPA^+ ions by smaller Na^+ ions causes exposition of a part of the terminal silanol groups to the liquid phase (see Schemes 1C1 and 1C2) and thus, makes them disposable for the formation of the ≡Si-O-Si≡ linkages between

the collided PNPs (see Eq. (1) and Scheme 1D). However, because of the "thick" shell, composed of polysilicate anions (oligomers) associated with TPA ions[52] (also see Scheme 2), the cores of the neighbouring PNPs cannot realize close contacts. By the same reason, the neighbouring PNPs are in aggregates bonded by limited number of ≡Si-O-Si≡ linkages (marked by the red ellipse in Scheme 2), realized through the exposed terminal sialon groups of nanoparticles shells. Both these factors ("separation" of cores and thus, absence of their coalescence from one side and limited number of the ≡Si-O-Si≡ linkages between the neighbouring PNPs in the aggregates from another side) make that the PNPs are not tightly bonded in the aggregates (see Scheme 2). This is the reason that the PNPs can be "plucked up" from the aggregates by chemically (action of OH^- ions), thermally (vibration and/or stretching) and/or mechanically (collisions of aggregates) induced breaking of ≡Si-O-Si≡ linkages between the PNPs. By the same reasons, about 10 nm-sized aggregates can be "plucked up" from the large about 1000 nm-sized aggregates. This leads to the assumption that the large particles represent low-density, rickety-held aggregates of the about 10 nm sized particles. Colloidal stability (absence of precipitation) and optical transparency of the HmRMs, containing the large aggregates, confirm this assumption. Hence, it is evident that the processes of aggregation and disaggregation are in dynamic equilibriums.

On the other hand, it is reasonable to assume that a part of the Na^+ ions associated with the deprotonated surface silanol groups (see Scheme 1C2) may penetrate deeper into nanoparticle shell or even into nanoparticle core as was already pointed out. In this case, the negative charge of the deprotonated surface silanol groups becomes uncompensated and may be again compensated by TPA^+ ions from solution, i.e., by these ones which were removed from the nanoparticle shell by the Na^+ ions, added in the HmRM, during the prolonged aging. In this way, the nanoparticle is stabilized again (see Scheme 1A), and thus, excluded from the processes of aggregation (see Scheme 1B). Since, as already is stated, the processes of

aggregation and disaggregation are in dynamic equilibrium, the excluded nanoparticles are replaced by the disaggregation of the larger aggregates.[52] By the same principle a disaggregation of large, about 1000 nm-sized aggregates to about 10 nm-sized ones can be explained (see Figs. S3, S4 and S5 and corresponding explanations in SI-2).

Comparison of the DLS-PSD curves in Figs. 1A, 1A' and 1B' show that the PNPs formed when NaOH was added directly (see Experimental), are stable for at least 24 h even when amount of the directly added NaOH is 15 times higher ($x_d \leq 0.027$, $R_d \leq 0.075$) than the amount of the subsequently added NaOH ($x_s = 0.0018$, $R_S = 0.005$; under this conditions the aggregation of the PNPs is immediate; see Fig. S2 in SI-2).

An increase of the amount of the directly added NaOH from $x_d = 0.027$ ($R_d = 0.075$) to $x_d = 0.036$ ($R_d = 0.1$) induces the aggregation of the PNPs (see Figs. S8 and S9 in SI-2) so that the size of the particles (aggregates) formed by the replacement of 10 mole % of TPAOH with directly added NaOH ($x_d = 0.036$, $R_d = 0.1$, $t_A = 24$ h) is almost the same as the size of the particles (aggregates) formed by the replacement of 1 mole % of TPAOH with subsequently added NaOH ($x_s = 0.0036$, $R_S = 0.01$) for $t_{A'} = 24$ h (compare Figs. 1C and 1C'). Prolonged *rt* aging causes further aggregation, so that particle (aggregate) size at $t_A \geq 8$ d is about ten times higher than at $t_A = 24$ h (see Fig. S9 in SI-2). For $x_d = 0.0396$ ($R_d = 0.11$), aggregation processes are very intense so that large aggregates [D_p(N) ≈ 100 nm] are formed at $t_s \leq 40$ min (see Fig. S10 in SI-2) and then the particle (aggregate) size slowly increases to D_p(N) ≈ 160 nm at $t_A \geq 24$ h (see Fig. 1D'; also see Fig. S10C in SI-2). Finally, for $x_d \geq 0.04142$ ($R_d = 0.13$), the PNPs immediately (at $t_s \leq 40$ min) aggregate to large [D_p(N) ≈ 700 nm] particles (aggregates) which size does not change during the prolonged *rt* ageing (see Figs. 1E' and 1F'; also see Fig. S11 in SI-3).

Similarly as in the case of the aggregates formed by subsequent addition of NaOH, the AFM cross section analysis (Fig. 2C') along the lines of the corresponding topographic 3D

height image (Fig. 2C) shows that the individual nanoparticles have a relative narrow height distribution ranging from about 1 to 2 nm and thus, that the particle size distribution, presented by the solid curves in Figs. 1C' – 1F', does not represent the distributions of individual (discrete) particles of different sizes but rather the aggregates of smaller, individual primary nanoparticles (PNPs).

Also, similarly as in the case of the subsequently added NaOH, the values of pH (and consequently, concentrations of OH^- ions) of the 2D-HmRMs aged at *rt* for t_A = 24 h, reached the „equilibrium“ values of $pH_{x,24h}$ and $[OH^-]_{x,24h}$ also in the case of directly added NaOH (see Table S1 in SI-1); again, the „equilibrium“ values do not considerably depend on $x = x_d$, because of the reasons explained in SI-1.

^{29}Si-NMR spectra of the selected 2D-HmRMs, prepared by direct addition of NaOH (2D-HmRMs; see Methods), are presented in Figs. 3D, 3E and 3F. From the already explained reasons, the results of their analyses (distribution of Si in the form of oligomers and distribution of S-O-Si connectives in nanoparticles) are presented in Tables S4 and S5 in SI-4, and some specific points are commented in SI-4.

Similarly as in the cases of subsequent addition of NaOH, direct addition of NaOH also causes appearance of broad bands in the range from $\delta \approx$ 1.5 ppm to $\delta \approx$ -1.5 ppm with the “peak” at about 0.2 ppm in the ^{23}Na NMR spectra presented in Figs. 4D – 4F. Hence, it indicates asymmetric environment of sodium ions as well.

On the basis of the presented results, only reasonable explanation for the observed effects is that for $x_d \leq 0.036$ ($R_d \leq 0.1$) almost complete amount of the directly added Na^+ ions are incorporated into nanoparticle core (see Schemes 3A - 3C) during its formation and before the formation of the nanoparticle shell. Thus, for $x_d \leq 0.036$, the amount of the Na^+ ions incorporated into nanoparticle core is proportional to x_d and R_d, respectively. However, a tendency of slow aggregation of the PNPs during prolonged *rt* ageing (see Figs. S8 and S9 in

SI-2) indicates that, even in these cases, small fractions of the directly added Na^+ ions participate in the removal the TPA^+ ions from the nanoparticle shell by the ion exchange process (see Schemes 1C and 3B) and thus, in the establishing of the ≡Si-O-Si≡ linkages between the collided PNPs, and formation of their aggregates [see Eq. (1) and Scheme 1D)].

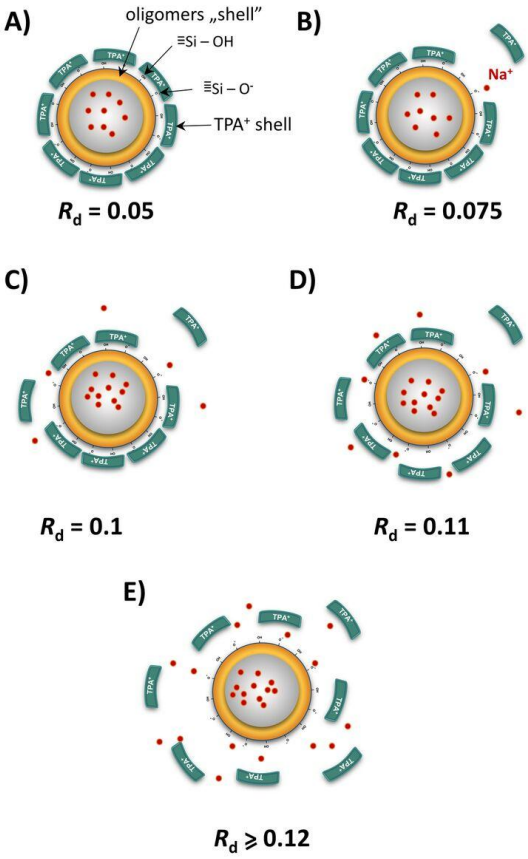

Scheme 3 Schematic presentation of the behaviour of primary nanoparticles (PNPs) in the 2D-HmRMs in which the increased amounts (from R_d = 0.05; A to $R_d \geq 0.12$; E) NaOH were added directly. Details are explained in the text.

The consequence is that the most of Na^+ ions are distributed in the nanoparticle core and part of them in on the nanoparticle shell, where exhibiting asymmetric environment shown by the broad lines in the corresponding ^{23}Na NMR spectra (Figs. 4D – 4F).

On the other hand, from the intense aggregation processes for $x_d > 0.036$ (see Figs. 1D' – 1F'; also see Figs S10 and S11 in SI-2), it is evident that $x_d = x_d(\mathrm{tr}) \approx 0.036$ ($R_d = R_d(\mathrm{tr}) \approx 0.1$) is a "threshold" amount of the Na^+ ions which can be incorporated into nanoparticle core and thus, that each „excess" ($x_d > 0.036$, $R_d > 0.1$) of the Na^+ ions acts as the subsequently added Na^+ ions (see Schemes 3D and 3E). Although the exact reason for this „threshold" amount of the directly added Na^+ ions is not quite clear at present, some probable reasons are considered in SI-2.

The incorporation of the directly added Na^+ ions into nanoparticle core can be explained by the fact that unlike to „large" TPA^+ ions which are not detected in nanoparticle core,[48] „small" Na^+ ions can be easily incorporated into nanoparticle core. However, it seems that this incorporation is not a simple entering of the hydrated „free" Na^+ ions into nanoparticle core during its formation, but rather the Na^+ ions are brought by the appropriate silicate species. Namely, it is known that Na^+ ions stabilize monomeric silicate species,[64] probably by formation of $Si(OH)_3O^-...^+Na$ species, i.e.,

$$Si(OH)_4 + OH^- + Na^+ \Longleftrightarrow Si(OH)_3O^-...^+Na + H_2O \qquad (2)$$

where $Si(OH)_4$ are silicate monomers formed during hydrolysis of TEOS [see Eq. (S4) in SI-2]. This implies that, at the critical aggregation concentration (CAC) of SiO_2,[21,27,47-49] there is a fraction of silicate species, in the form of $Si(OH)_3O^-...^+Na$, which is proportional to the amount, x_d, of the directly added NaOH. Now, taking into consideration the finding that reactions between single-charged and neutral silicate species are favoured over those involving either two neutral or two charged silicate species,[65] it is reasonable to conclude that the reaction of the $Si(OH)_3O^-...^+Na$ species, formed below the CAC, with the $Si(OH)_4$ monomers, formed above the CAC[21,27,48] (see also SI-1), is the dominant process at the early

stage of the formation of nanoparticle core. This is, at the same time, the obvious reason that the Na^+ ions are incorporated to the nanoparticle core. At prolonged hydrolysis of TEOS, above the CAC, the formation of nanoparticles can be governed by either addition of monomers[66] or by aggregation of all types of oligomers,[49] or what is also reliable, that both these processes occur simultaneously.

The presented results clearly show that a controlled addition of NaOH, with respect to its amount (x, *R*) and mode of its addition (subsequent, direct), results in the formation of silica particles (aggregates) of different sizes (in the range from about 1 nm to about 1000 nm) containing or not, different amount of Na^+ ions in the nanoparticle core. Interestingly, regardless to the mode of NaOH addition (subsequent or direct) and the values of x (x_s, x_d) and R (R_s, R_d), the larger particles formed, by Na^+-initiated aggregation of the PNPs do not appear as the single (individual) particles, but as aggregates of smaller ones (1 – 2 nm), shown in the AFM 3D-height images in Figs. 2B and 2C.

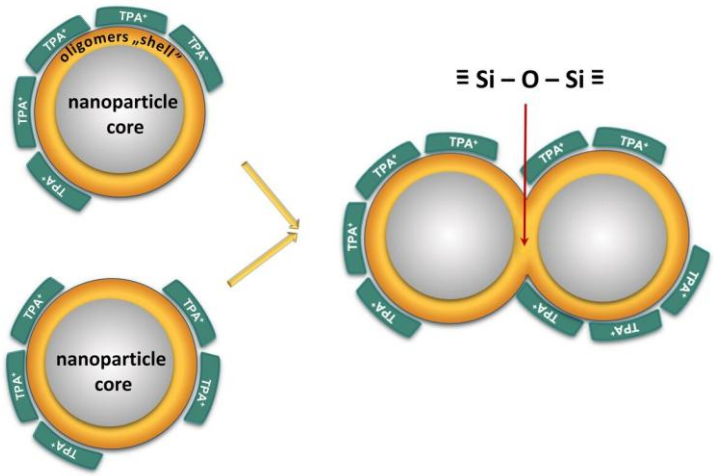

Scheme 4 Schematic presentation of the primary nanoparticles (PNPs) bonded by ≡Si-O-Si≡ linkages through the "oligomers shells" (see details in Scheme 2), after effective collision of the PNPs in which a part of the TPA^+ ions from the shells is removed by action of the subsequently added Na^+ ions. Details are explained in the text.

The absence of coalescence of the participated (linked) PNPs (see Schemes 1D and 4) may be explained by preventing a direct contacts of the nanoparticles cores, caused by the presence of polysilicate anions (oligomers) in the nanoparticle shell (see Schemes 2 and S1 in SI-3). On the other hand, this implies that the coalescences of the linked PNPs would be possible in the cases when the nanoparticle shell is tenuous enough to allow close contacts between the nanoparticles cores. It has been found recently that a small fraction of $Si(OH)_4$ monomers, formed during the hydrolysis of TEOS, participates in the formation of the core(amorphous silica)@shell(TPA^+ ions) nanoparticles (PNPs), below the CAC.[52] Similarly to the core(amorphous silica)@shell(TPA-polysilicates) nanoparticles, formed above the CAC (see Schemes 1A, 1B and 1C1; see also Scheme S1 in SI-3), the nanoparticles formed below the CAC are stabilized electrostatically[31,35,50,60] and sterically.[8,29,50,60,61]

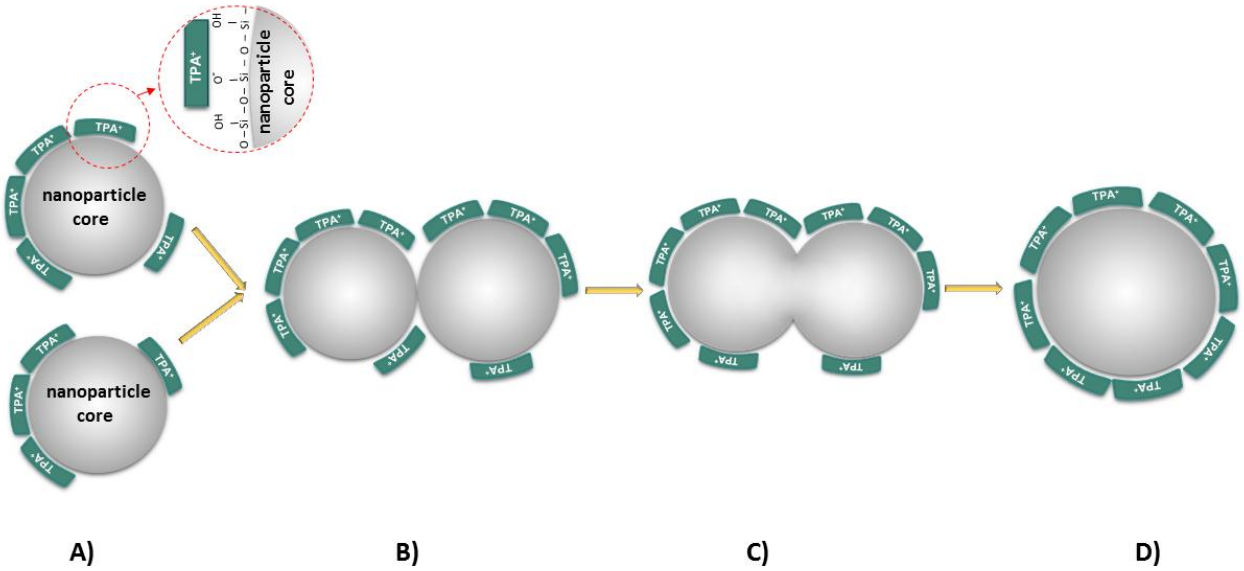

Scheme 5 Schematic presentation of: (A) The primary nanoparticles (PNPs), formed below the CAC, after subsequent addition of NaOH. (B) Formation of aggregates of the PNPs after their successful collision and formation of ≡Si-O-Si≡ linkages between the nanoparticles cores. (C) and (D) Coalescence of the nanoparticles cores and formation of larger nanoparticle. Details are explained in the text

In both cases, the steric stabilization is enabled by overlapping the terminal silanol groups with TPA^+ ions and thus by preventing the formation of ≡Si-O-Si≡ bridges between the collided PNPs [see Eq. (1) and Schemes 1B and 1E]. While in the nanoparticles formed above the CAC, the TPA^+ ions are associated with the deprotonated terminal silanol groups of the polysilicate anions[52] (see Schemes 1 – 3; see also Scheme S1 in SI-3), in the nanoparticles formed below the CAC, the TPA^+ ions are associated with the deprotonated surface silanol groups of the nanoparticle core[52] (see Scheme 5A).

Following the processes which occur when NaOH is subsequently added to the 1a-HmRMs, prepared above the CAC (see Scheme 1), one can assume that the subsequent addition of NaOH to the 1b-HmRMs, prepared below the CAC, would induce the same processes, i.e., partial or entire exchange of the TPA^+ ions from the nanoparticles shells with smaller Na^+ ions (see Scheme 5A) and aggregation of the nanoparticles by formation of the ≡Si-O-Si≡ linkages between the nanoparticles cores (see Scheme 5B). However, while the "large" shells, composed of polysilicate anions (oligomers) associated with TPA ions[52] (also see Scheme 2), prevent the close contacts between the cores of the nanoparticles formed above the CAC and thus, their coalescences (see Schemes 1D and 4), one can assume that the close contacts between the cores of the nanoparticles formed below the CAC (see Scheme 5B), allow their coalescences into larger single spherical nanoparticles[67,68] (see Schemes 5C and 5D). To prove (or disapprove) this assumption, we analysed by different methods (^{29}Si-NMR, ^{23}Na-NMR, DLS and AFM) both the NaOH-free 1b-HmRM: $0.2SiO_2$:0.3528TPAOH:0.8EtOH:18.05H_2O and Na-containing 1bS-HmRM: $0.2SiO_2$:0.0072NaOH:0.3528TPAOH:0.8EtOH:19.46H_2O (see Experimental).

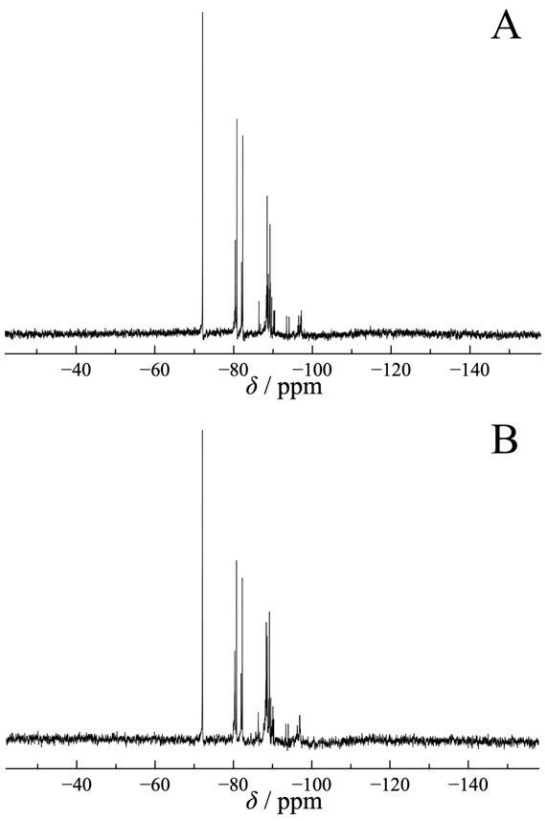

Fig. 5 ^{29}Si-NMR spectra of the 1b-HmRM: $0.2SiO_2$:0.3528TPAOH:0.8EtOH:18.05H_2O (A) and 1bS-HmRM: $0.2SiO_2$:0.0072NaOH:0.3582TPAOH:0.8EtOH:19.6H_2O (B), prepared and treated as it is described in Experimental.

Figure 5 shows that the ^{29}Si-NMR spectra of both NaOH-free 1b-HmRM and NaOH-containing 1bS-HmRM exhibit only the sharp lines characteristic of small dissolved silicate oligomers (see Table S6 in SI-4), as it is specific for the HmRMs prepared below the CAC (OH^-/SiO_2 = 1.8 > 1).[21,27,30,34,47,48,49,50] Because of the absence the broader bands, silica nanoparticles cannot be detected in the corresponding ^{29}Si-NMR spectra (Fig. 5), which is consistent with the results of previous studies.[15,16,21,30,49,51,52] The most possible reason is very small amount (fraction) of silica present in eventually formed nanoparticles, which is below the detection limit of the applied method (see Experimental). On the other hand, since DLS[52,69] and AFM[52] detect the presence of nanoparticles with higher sensitivity than any other methods, the 1b-HmRM and 1bS-HmRM were analysed by DLS and, additionally by AFM.

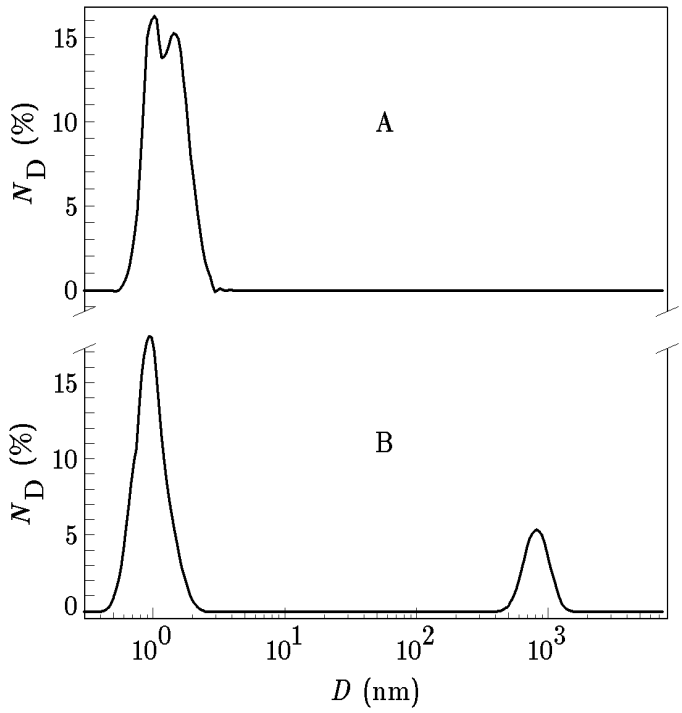

Fig. 6 DLS-PSD by number of the 1b-HmRM: $0.2SiO_2$:0.3528TPAOH:0.8EtOH:$19.6H_2O$ (A) and 1bS-HmRm: $0.2SiO_2$:0.0072NaOH:0.3582TPAOH:0.8EtOH:$19.6H_2O$ (B), prepared and treated as it is described in Experimental. N_D is the number percentage of the particles having the spherical equivalent diameter D.

Particle size distribution curve by number in Fig. 6A shows that the NaOH-free 1b-HmRM, stirred/aged at *rt* for $t_A = t_s + t_a = 24$ h (see Experimental), contains the "particles" having the size in the range from $D_{min} = 0.4$ nm to $D_{max} = 2.33$ nm with peak sizes D_p(I) = 0.72 nm and D_p(II) = 1.3 nm. On the basis of previous studies is estimated that the features smaller than 1 nm, possibly correspond to the polysilicate anions (oligomers) associated with TPA^+ ions or even the core@shell particles at the early stage of formation,[51,52] and that the particles having the size $D \geq 1$ nm, represent primary, core(amorphous silica)@shell(TPA^+ ions), nanoparticles.[52]

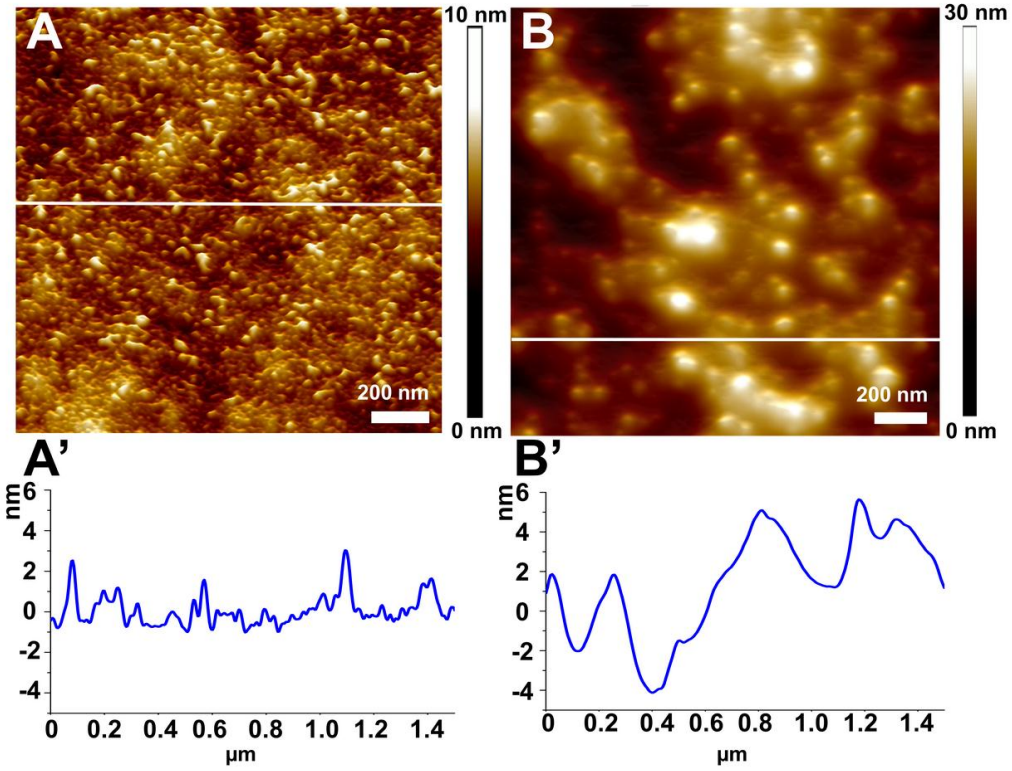

Fig. 7 AFM topographic height images (A, B) and the corresponding section analyses (A', B') of the nanoparticles in the 1b-HmRMs: $0.2SiO_2$:0.3582TPAOH:0.8EtOH:$19.6H_2O$ (A, A') and 1bS-HmRM: $0.2SiO_2$:0.0072NaOH:0.3528TPAOH:0.8EtOH:$19.6H_2O$ (B, B'), prepared and treated as it is described in Experimental. Images are presented as 3D height data (A, B) and the cross-section through the line shown on the same scale (A', B'): scan size of 1400 nm × 1400 nm and vertical scale of 10 nm (A) and 30 nm (B)

The presence of the nanoparticles in 1b-HmRM is confirmed by AFM visualization. The AFM topographic height image in Fig. 7A clearly shows that the single (individual) nanoparticles are deposited on mica surface during the preparation of samples for the AFM imaging (see Experimental). The AFM cross-section analysis (Fig. 7A'), along the line of the corresponding topographic height image of the surface layer of nanoparticles on mica support, shows that the nanoparticles heights lie in the range from about 1 nm to about 3 nm, which is consistent with the results of the DLS analysis.

Subsequent addition of NaOH into NaOH-free HmRM (1b-HmRM; see Experimental) causes formation of the population of sub-micrometre to micrometre sized particles, having the sizes in the range from D_{min} = 420 nm to D_{max} = 1400 nm with D_p = 825

nm (Fig. 6B), in the Na-containing 1bS-HmRM. On the other hand, the AFM visualization of the particles present in 1bS-HmRM shows that the large particles do not represent aggregates of the PNPs, as it is characteristic for the HmRMs prepared above the CAC (see Figs, 2B, 2B', 2C and 2C'), but that the large particles are composed of discrete (individual) nanoparticles (Fig. 7B) having the size in the range from 4.6 – 12.6 nm, as it is estimated by the cross-section analysis (Fig. 7A').

On the basis of the results presented in Figs. 6 and 7 is evident that addition of Na^+ ions into NaOH-free HmRM (1b-HmRM -> 1bS-HmRM; see Experimental) causes aggregation of a part of the primary core(amorphous silica)@shell(TPA^+ ions) nanoparticles formed in 1b-HmRM. It is reasonable to conclude that this is realized in the same way as in the HmRMs formed above the CAC. However, while the aggregates formed in the 1aS-HmRMs and 2D-HmRMs, prepared above the CAC are, by already explained reason, composed of discrete (individual) PNPs (see Figs. 2B, 2B', 2C and 2C'), the large particles (aggregates) formed in the 1bS-HmRM), prepared below the CAC (see Fig. 6B), are composed of the particles larger than PNPs (see Figs 7B and 7B'). Hence, it is evident that close contacts between the cores of the PNPs formed below the CAC enable their coalescence into larger individual nanoparticles (see Schemes 5C and 5D). This undoubtedly indicates that the process of aggregation is accompanied with coalescences of the PNPs into larger individual nanoparticles (see Schemes 5C and 5D) and thus, confirms the prediction that in the nanoparticles formed below the CAC, the TPA^+ ions are associated with the deprotonated surface silanol groups of the nanoparticle core[52] (see Scheme 5A). At the same time, this confirms the conclusion that in-feasibleness of coalescences of the PNPs in their aggregates (see Figs. 2B, 2B', 2C and 2C'), formed above the CAC, is caused by separation of the nanoparticles cores by the shells composed of polysilicate anions[52] (see Schemes 2 and 4).

Conclusions

The influence of the amount of Na^+ ions, added as NaOH into homogeneous reaction mixtures (HmRMs) during (direct addition) and/or after formation of the core@shell silica primary nanoparticles (PNPs) (subsequent addition) at room temperature (*rt*), on the processes of their aggregation at *rt*, and on the characteristics of the obtained aggregates, was investigated. Analyses of the obtained results showed that:

(1) The primary silica nanoparticles (PNPs), formed at *rt* in the NaOH-free homogeneous reaction mixture ($HmRM_0$-I: SiO_2:0.36TPAOH:4EtOH:18H_2O), have the size (spherical equivalent diameter, *D*) in the range from about 1 nm to about 3.5 nm and are, at *rt*, stable for a long time (at least 37 days in our case).

(2) The Na^+ ions, subsequently added into NaOH-free HmRMs [SiO_2:(0.36–x_s)TPAOH: 4EtOH:(18–y)H_2O + x_sNaOH + $y$$H_2O$ -> SiO_2:x_sNaOH:(0.36–x_d)TPAOH:4EtOH:18H_2O] remove the TPA^+ ions from the PNP's shell by the ion exchange process. This process causes exposition of a part of the terminal silanol groups and thus, enables the formation of the ≡Si-O-Si≡ linkages between the neighbouring PNPs, after the efficient collisions. This results in the formation of the nanoparticles larger than PNPs.

(3) The Na^+ ions, present in the 2D-HmRM: SiO_2:x_dNaOH:(0.36–x_d)TPAOH:4EtOH:18H_2O during the formation of the PNPs (directly added NaOH) are associated with the deprotonated monomers [$Si(OH)_3O^{-\cdots+}Na$], formed below the CAC. These associates react with protonated monomers [$Si(OH)_4$], formed above the CAC, as the initial step of the formation of the nanoparticle core. In this way, Na^+ ions are incorporated into nanoparticle core before the formation of shell. However, because there is a threshold amount, $x_d(tr) \approx 0.036$, of the Na^+ ions that can be incorporated to the nanoparticle core,

each „excess“ (x_d > 0.036) of the Na^+ ions acts as the subsequently added Na^+ ions [see (2)]. The consequence is that achieving of given effects (rate of the nanoparticles enragement and the final particle size) requires considerably larger amount of the directly added NaOH than the subsequently added NaOH.

(4) The presented results clearly show that a controlled addition of NaOH, with respect to its amount (x, *R*) and mode of its addition (subsequent, direct), results in the formation of silica particles with different sizes (in the range from about 1 nm to about 1000 nm) containing or not, different amount of Na^+ ions in the particle core.

(5) The populations of the particles larger than PNPs do not represent individual (discrete) particles of different sizes, as it is measured by DLS, but represent aggregates of individual PNPs, as it is determined by AFM. This indicates that the cores of the individual PNPs in aggregates are not in close contacts, but that are separated by the nanoparticles shells, composed of polysilicate anions (oligomers).

(6) Although the silica nanoparticles cannot be detected by ^{29}Si-NMR in the NaOH-free HmRM, prepared below the CAC, DLS and AFM analyses of the 1bS-HmRM: $0.2SiO_2$:0.0072NaOH:0.3582TPAOH:0.8EtOH:$19.6H_2O$, formed by subsequent addition of NaOH solution into NaOH-free 1b-HmRM: $0.2SiO_2$:0.3582TPAOH:0.8EtOH:$18.05H_2O$ showed that: (i) part of the PNPs ($D \approx 1 - 3$ nm), formed in NaOH-free 1b-HmRM “transforms” into population of particles having the sizes in the range from D_{min} = 420 nm to D_{max} = 1400 nm, as it was measured by DLS, (ii) the large particles represent aggregates composed of the particles having the size in the range from 4.6 – 12.6 nm, as it is estimated by AFM height imaging and corresponding cross-section analysis. This undoubtedly indicates that the process of aggregation is, because of the close contacts of the PNPs cores, accompanied with coalescences of the PNPs into larger individual nanoparticles and thus, confirm the

prediction that in the nanoparticles formed below the CAC, the TPA^+ ions are associated with the deprotonated surface silanol groups of the nanoparticle core.

Conflict of interest

There are no conflicts to declare.

Acknowledgements

This work is by Croatian Science Foundation, under project IP-2016-06-2214 and IP-2016-06-8415. Author V.S. received funding for equipment from the Ministry of Science and Education of the Republic of Croatia.

Supporting Information

The Supporting Information (SI) is available free of charge on the ACS Publications website.

References

1 R. M. Barrer, *Hydrothermal Chemistry of Zeolites*, Academic Press, London and New York, 1982, pp 133-247.
2 L. C. Boudreau, J. A. Kuck and M. Tsapatsis, *J. Membr. Sci*., 1999, **152**, 41-59.
3 B. J. Schoeman, J. Sterte and J.-E. Otterstedt, *Zeolites*, 1994, **14**, 110-116.
4 A. E. Persson, B. J Schoeman, J. Sterte and J.-E. Otterstedt, *Zeolites*, 1995, **15**, 611-619.
5 B. J. Schoeman, *Zeolites*, 1997, **18**, 97-105.
6 B. J. Schoeman, *Stud. Surf. Sci. Catal*., 1997, **105,** 647-654.
7 B. J. Schoeman, J. Sterte and J.-E. Otterstedt, *Zeolites*, 1994, **14,** 208-216.
8 B. J. Schoeman, *Microporous Mesoporous Mater*., 1998, **22,** 9-22.
9 G. Zhu, S. Qiu, J. Yu, Y. Sakamoto, F. Xiao, R. Xu and O. Terasaki, *Chem. Mater.*, 1998, **10,** 1483-1486.
10 S. Mintova, N. H. Olson, V. Valtchev and T. Bein, *Science*, 1999, **283,** 958-960.
11 V. Valtchev and S. Mintova, *Microporous Mesoporous Mater*., 2001, **43,** 41-49.
12 Y. Hu, C. Liu, N. Ren and Y. Tang, *Microporous Mesoporous Mater*., 2009, **119,** 306-314.
13 R. Li, N. Linares, J. G. Sutjianto, A. Chawla, J. Garcia-Martinez and J. D. Rimer, *Angew. Chem. Int. Ed. Engl*., 2018, **57,** 11283-11288.
14 J.-S. Wu, A. S. T. Chiang and T.-C. Tsai, *Sci. Adv. Mater*., 2011, **3,** 1011-1018.
15 N. Hould, M. Haouas, V. Nikolakis, F. Taulelle and R. Lobo, *Chem. Mater*., 2012, **24,** 3621-3632.
16 M. Castro, M. Haouas, I. Lim, H. J. Bongard, F. Schüth, F. Taulelle, G. Karlsson, V.

Alfredsson, E. Breyneart, C. E. A. Kirschhock and W. Schmidt, *Chem. – Eur. J.*, 2016, **22,** 15307-15319.
17 N. D. Hould and R. F. Lobo, *Chem. Mater.*, 2008**, 20,** 5807–5815.
18 S. Mintova, S. Mo and T. Bein, *Chem. Mater*., 1998, **10,** 4030-4036.
19 S. Mintova, N. Petkov, K. Karaghiosoff and T. Bein, *Microporous Mesoporous Mater*., 2001, **50,** 121-128.
20 E.-P. Ng, D. Chateigner, T. Bein, V. Valtchev and S. Mintova, *Science*, 2012, **335,** 70-73.
21 E. A. Eilertsen, M. Haouas, A. B. Pinar, N. D. Hould, R. F. Lobo, K. P. Lillerud and F. Taulelle, *Chem. Mater*., 2012, **24,** 571-578.
22 N. Ren, Z.-J. Yang, X.-C. Lv, J. Shi, Y.-H. Zhang and Y. A. Tang, *Microporous Mesoporous Mater.*, 2010, **131,** 103-114.
23 W. H. Dokter, H. F. van Garderen, T. P. M. Beelen, R. A. van Santen and W. Bras, *Angew. Chem., Int. Ed. Engl.*, 1995, **34,** 73-75.
24 J. N. Watson, L. E. Iton, R. I. Keir, J. C. Thomas, T. L. Dowling and J. W. White, *J. Phys. Chem. B*, 1997, **101,** 10094-10104.
25 P.-P. E. A. de Moor, T. P. M. Beelen, B. U. Komanschek, L. W. Beck, P. Wagner, M. E. Davis and R. A. van Santen, *Chem. - Eur. J.*, 1999, **7,** 2083-2088.
26 S. Mintova, N. H. Olson, J. Senker and T. Bein, *Angew. Chem., Int. Ed. Engl.*, 2002, **41,** 2558-2561.
27 J. D. Rimer, G. D. Vlachos and R. F. Lobo, *J. Phys. Chem. B*, 2005, **109,** 12762-12771.
28 C.-H. Cheng and D. F. Schantz, *Curr. Opin. Colloid Interface Sci.*, 2005, **10,** 188-194.
29 T. M. Davis, T. O. Drews, H. Ramanan, C. He, J. Dong, H. Schnablegger, M. A. Katsoulakis, E. Kokkoli, A. V. McCormick, R. L. Penn and M. Tsapatsis, *Nat. Mater*., 2006, **5,** 400-408.
30 A. Aerts, M. Haouas, T. P. Caremans, L. R. A. Follens, T. S. van Erp, F. Taulelle, J. Fermant, J. A. Martens and C. E. A. Kirschhock, *Chem. - Eur. J.*, 2010, **16,** 2764-2774.
31 V. Nikolakis, E. Kokkoli, M. Tirrell, M. Tsapatsis and D. G. Vlachos, *Chem. Mater*., 2000, **12,** 845-853.
32 C.-H. Cheng and D. F. Shantz, *J. Phys. Chem. B*, 2005, **109,** 13912-13920.
33 S. Mintova, V. Valtchev and T. Bein, *Colloids and Surfaces A: Pysicochem. Eng. Aspects*, 2003, **217,** 153-157.
34 S. Yang and A. Navrotsky, *Chem. Mater*., 2004, **16,** 3682-3687.
35 J. D. Rimer, J. M. Fedeyko, D. G. Vlachos and R. F. Lobo, *Chem. - Eur. J.*, 2006, **12,** 2926-2934.
36 P.-P. E. A. de Moor, T. P. M. Beelen, B. U Komanschek, O. Diat and R. A van Santen, *J. Phys. Chem. B*, 1997, **101,** 11077-11086.
37 V. Nikolakis, M. Tsapatsis and D. G. Vlachos, *Langmuir*, 2003, **19,** 4619–4626.
38 T. A. M. Twomey, M. Mackay, H. P. C. E. Kuipers and R. W. Thompson, *Zeolites*, 1994, **14,** 162-168.
39 D. Liang, L. R. A. Follens, A. Aerts, J. A. Martens, G. Van Tendeloo and C. E. A. Kirschhock, *J. Phys. Chem. C*, 2007, **111,** 14283-14285.
40 O. Regev, Y. Cohen, E. Kehat and Y. Talmon, *Zeolites*, 1994, **14,** 314-319.
41 C. D. Chang and A. T. Bell, *Catal. Lett*., 1991, **8,** 305–316.
42 S. L. Burkett and M. E. Davis, *J. Phys. Chem*., 1994, **98,** 4647-4653.
43 A. Čižmek, B. Subotić, D. Kralj, V. Babić-Ivančić and A. Tonejc, *Microporous Mater.*, 1997, **12,** 267-280.
44 C. Kosanović, K. Havenscak, B. Subotić, V. Svetličić, T. Mišić, A. Cziraki and G. Huhn, *Microporous Mesoporous Mater.*, 2009, **123,** 150-159.

45 N. Ren, S. Bosnar, J. Bronić, M. Dutour Sikirić, T. Mišić, V. Svetličić, J.-J. Mao, T. Antonić Jelić, M. Hadžija and B. Subotić, *Langmuir*, 2014, **30,** 8570-8579.
46 L. R. A. Follens, A. Aerts, M. Haouas, T. P. Caremans, B. Loppinet, B. Goderis, J. Vermant, F. Taulelle, J. A. Martens and C. E. A. Kirschhock, *Phys. Chem. Chem. Phys*., 2008, **10,** 5574-5583.
47 J. M. Fedeyko, J. D. Rimer, R. F. Lobo and D. G. Vlachos, *J. Phys. Chem. B*, 2004, **108,** 12271-12275.
48 J. M. Fedeyko, D. G. Vlachos and R. F. Lobo, *Langmuir*, 2005, **21,** 5197-5206.
49 D. P. Petry, M. Haouas, S. C. C. Wong, A. Aerts, C. E. A. Kirschhock, J. A. Martens, S. J. Gaskell, M. W. Anderson and F. Taulelle, *J. Phys. Chem. C*, 2009, **113,** 20827-20836.
50 J. D. Rimer, R. F. Lobo and D. G. Vlachos, *Langmuir*, 2005, **21,** 8960-8971.
51 T. P. Caremans, B. Loppinet, L. R. A. Follens, T. S. van Erp, J. Vermant, B. Goderis, C. E. A. Kirschhock, J. A. Martens, and A. Aerts, *Chem. Mater*., 2010, **22,** 3619-3629.
52. S. Bosnar, T. Antonić Jelić, J. Bronić, M. Dutour Sikirić, S. Šegota, V. Čadež, V. Smrečki, A. Palčić, and B. Subotić, *J. Phys. Chem. C*, 2018, **122,** 9441-9454.
53. M. Jorge, S. M. Auerbach and P. A. Monson, *J. Am. Chem. Soc*., 2005, **127,** 14388−14400.
54. S. M. Auerbach, M. H. Ford and P. A. Monson, *Curr. Opin. Colloid Interface Sci*., 2005, **10,** 220−225.
55. S.-C. Chien, S. M. Auerbach and P. A. Monson, *Langmuir*, 2015, **31,** 4940−4949.
56. A. Rivas-Cardona, M. Chovanetz and D. F. Shantz, *Microporous Mesoporous Mater*., 2012, **155,** 56-64.
57. S. D. Kinrade, C. T. G. Knight, D. L. Pole, and R: T: Syvitski, *Inorg. Chem*., 1998, **37,** 4278-4283.
58. C. O. Metin, L. W. Lake, C. R. Miranda and Q. P. Nguyen, *Nanoparticle Res*., 2011, **13,** 839-850.
59. D. Massiot, F. Fayon M. Capron, I. King, S. Le Calvé, B. Alonso, J. O. Durand, B. Bujoli, Z. Gan and G. Hoatson, *Magn. Reson. Chem.*, 2002, **40,** 70-76.
60. S. Yang, A. Navrotsky, D. J. Wesolowski and J. A. Pople, *Chem. Mater.*, 2004, **16,** 210-219.
61. N. D. Hould, A. Foster and R. F. Lobo, *Microporous Mesoporous Mater*., 2011, **142,** 104-115.
62. J. M. Fedeyko, H. Eglof-Fox, D. W. Fickel, D. G. Vlachos and R. F. Lobo, *Langmuir*, 2007, **23,** 4532-4540.
63. X. Xue and J. F. Stebbibs, *Phys. Chem. Miner.*, 1993, **20,** 297-307.
64. I. Hasegawa, S. Sakka, K. Kuroda and C. Kato, *Bull. Inst. Chem. Res. Kyoto Univ*., 1987, **65,** 192-196.
65. M. J. Mora-Fonz, C. R. A. Catlow and D. W. Lewis, *Angew. Chem. Int. Ed*., 2005, **44,** 3082-3086.
66. J. L. Provis and D. G. Vlachos, *J. Chem. Phys. B*, 2006, **110,** 3098-3108.
67. H. Nishimori, M. Tatsumisago and M. Tsutomu, *J. Sol-Gel Sci. Technol*., 1997, **9,** 25-31.
68. T. Hawa and M. R. Zachariah, *J. Aerosol Sci*., 2006, **37,** 1-15.
69. M. Castro, M. Haouas, F. Taulelle, I. Lim, E. Breynaert, G. Brabants, C. E. A. Kirschhock

and W. Schmidt, *Microporous Mesoporous Mater*., 2014, **189,** 158-162.